

The BHSD Dataset: A 3D Brain Hemorrhage Segmentation Dataset with multi-class and multi-annotated information

Biao Wu¹, Yutong Xie¹, Zeyu Zhang^{1,3}, Jinchao Ge¹, Kaspar Yaxley², Suzan Bahadir², Qi Wu¹, Yifan Liu^{1,4}, and Minh-Son To²

¹ Australia Institute of Machine Learning, University of Adelaide

² Flinders Health and Medical Research Institute, Flinders University

³ Australian National University

⁴ ETH Zürich

Abstract. Intracranial hemorrhage (ICH) is a pathological condition characterized by bleeding inside the skull or brain, which can be attributed to various factors. Deep learning techniques are widely used in medical image segmentation, and part of the brain haemorrhage segmentation task has been initially implemented by way of annotated data. However, existing public ICH datasets are inadequate for multi-class segmentation tasks. To overcome this, we develop the Brain Hemorrhage Segmentation Dataset (BHSD), which provides a 3D multi-class ICH dataset containing 200 volumes with pixel-level annotations and 2200 volumes with slice-level annotations across five categories of ICH. Subsequently, we formulate three progressive tasks based on the established benchmark, including supervised, semi-supervised, and semi-weakly supervised ICH segmentation. Additionally, we present experimental results using advanced supervised and semi-supervised segmentation models as reference benchmarks. These results can serve as a starting point for further model development and evaluation of the BHSD dataset. The dataset and checkpoint is available at <https://github.com/White65534/BHSD>.

Keywords: Intracranial hemorrhage · Segmentation · Multi-class.

1 Introduction

Intracranial hemorrhage (ICH) describes bleeding inside the skull or brain and encompasses a variety of different bleeds. The key types of ICH, based on the anatomical relation of the bleed with the brain and membranes surrounding the brain (meninges), are extradural hemorrhage (EDH), subdural hemorrhage (SDH), subarachnoid hemorrhage (SAH), intraparenchymal hemorrhage (IPH), and intraventricular hemorrhage (IVH). There are a number of causes of ICH [9,5,17], including trauma, vascular malformations, tumours, hypertension and venous thrombosis. Suspected ICH is commonly evaluated with a non-contrast CT scan, which can reveal the type of bleed and distribution of blood.

Acute blood on CT appears hyperdense, relative to brain matter, while chronic blood products appear hypodense. Automated hemorrhage detection can expedite management and intervention, while volumetric quantification of bleeding patterns enables clinicians to estimate severity, predict outcomes, and monitor progress [19,8,1]. Meantime, the rapid development of deep learning also has accelerated the development of automated segmentation of ICH regions using annotated data to train models [24,14].

Existing public ICH datasets are either focused on hemorrhage classification or single-class hemorrhage segmentation, *i.e.*, foreground or background, hence these are not adequate for the multi-class segmentation problem. Therefore, the purpose of this work is to leverage the existence of a large, public ICH dataset to produce a 3D multi-class ICH segmentation dataset with pixel-level hemorrhage annotations, hereafter referred to as the brain hemorrhage segmentation dataset (BHSD). We demonstrate the utility of this dataset by performing three series of experiments: (1) supervised ICH segmentation with advanced backbones, (2) semi-supervised ICH segmentation with labeled and unlabeled data, and (3) semi-weakly supervised ICH segmentation with labeled and weakly-labeled data. These experiments prove the feasibility of performing multi-class segmentation on ICH imaging and provide a benchmark for subsequent related work.

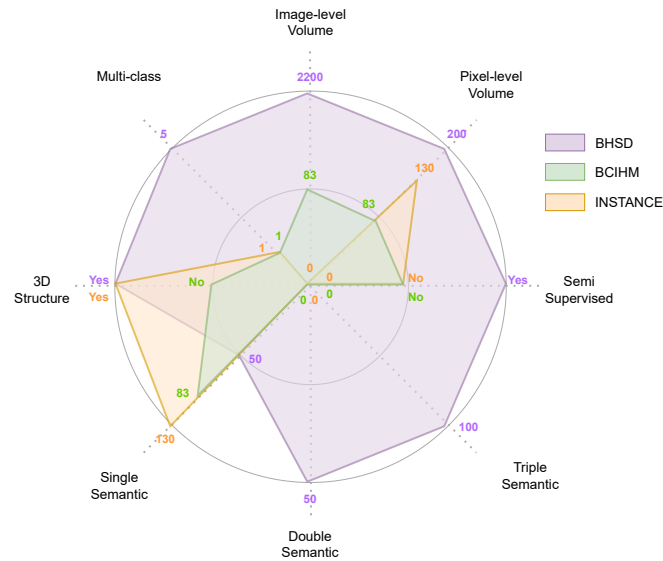


Fig. 1. Comparison of the BCIHM dataset, INSTANCE dataset and BHSD in terms of data characteristics. BHSD provides more data, and more annotation information with different levels, which offers a valuable resource for developing and testing new machine learning algorithms for ICH segmentation.

2 The BHSD Dataset

Deep learning has stimulated an explosion in computer vision applications in medical imaging, leading to the emergence of various datasets aimed at enhancing brain hemorrhage segmentation, including computed tomography (CT) images for intracranial hemorrhage detection and segmentation dataset (BCIHM) [10] and the INSTANCE dataset [15]. The BCIHM dataset, which was released on the Kaggle platform in 2019, comprises 83 volumes and supports only foreground and background segmentation. Furthermore, images in this dataset are provided in PNG format, which is not appropriate for extracting structural (*i.e.*, 3D) information. In contrast, the INSTANCE dataset, introduced as part of a MICCAI 2022 Challenge, consists of 200 volumes, of which 130 have foreground and background segmentation labels. The volumes in this dataset are provided in NIfTI format, but only with a single bleed in each slice.

Differentiating between various categories of ICH is crucial, as treatment options may vary depending on the type of bleed. Unfortunately, current datasets such as the BCIHM and INSTANCE datasets, only support binary segmentation for the presence of bleed, lacking the fine-grained hemorrhage segmentation. This limitation served as the impetus for developing the BHSD. Unlike the BCIHM and INSTANCE datasets, the BHSD includes images with varying numbers of hemorrhages, ranging from none to as many as five different types. Despite being more challenging, our multi-class segmentation dataset aligns more closely with the clinical reality of managing brain hemorrhage [11].

This paper provides a large-scale BHSD dataset with high-quality annotations on 5 types of brain bleeds. The BHSD comprises 3D CT head scans, some with hemorrhages and others without. 200 scans have pixel-level annotations with one of five categories of ICH: epidural, intraparenchymal, intraventricular, subarachnoid, or subdural. The annotations were performed by three medical imaging experts to ensure label precision and quality. The images in our BHSD dataset are collected from the Radiological Society of North America (RSNA) dataset [4] and subsequently relabeled with multi-class pixel-level annotations. This dataset is a public collection of 874 035 CT head images from a mixed patient cohort with and without ICH. And it is multi-institutional and multi-national and includes image-level expert annotations from neuroradiologists about the presence and type of bleed. This dataset was used for the RSNA 2019 Machine Learning Challenge for detecting brain hemorrhages, *i.e.*, a classification, not segmentation problem [4]. We also collected the corresponding image-level annotations from the RSNA dataset. By covering both image-level and pixel-level annotations, our BHSD dataset offers a more comprehensive understanding of the imaging data, contributing to the development of more accurate and effective deep learning methods models for ICH segmentation.

2.1 Dataset collection and annotation

The BHSD is a high-quality medical imaging dataset comprising 2200 high-resolution 3D CT scans of the brain, each containing 24 to 40 slices of 512×512

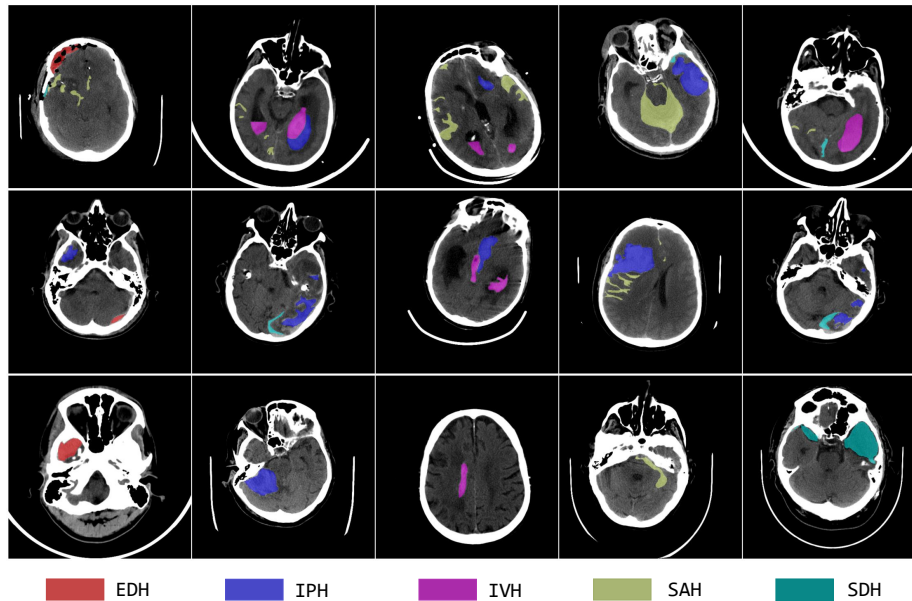


Fig. 2. The BHSD contains five hemorrhage categories and includes cases where multiple bleeds are present in a volume. Annotations for a single hemorrhage represent 25% of the total annotations, those for a double hemorrhage represent 25% of the total annotations and those for a three or more hemorrhages represent 50% of the total annotations. The different colours in the figure correspond to a specific category

pixels. As the RSNA dataset was provided in DICOM format, with anonymised patient identifiers while retaining geometric data, the original 3D head scans could be reconstructed and converted to NIfTI format [13]. Hemorrhages on individual head scans were segmented using ITK-SNAP [27] by two trained medical imaging experts, using the original image-level annotations provided with the RSNA dataset as a guide. These annotations were then reviewed by a board-certified radiologist, ensuring the quality of the annotations. In addition to the 200 volumes with pixel-level annotations, a further 2000 head scans were reconstructed with image-level annotations.

2.2 Application on BHSD

In this section, we describe three segmentation tasks designed to leverage the proposed BHSD.

Task 1: Supervised segmentation with advanced benchmarks. Supervised multi-class segmentation refers to the classification of all individual pixels in an image into distinct classes, using segmentation mask annotations for supervision. In the task of segmenting ICH, multi-class segmentation has greater significance and challenge compared with foreground and background

segmentation. Multi-class segmentation can more accurately identify and segment different types of ICH, which is important for diagnosis, treatment and prognostic evaluation. Meanwhile, multi-class segmentation can improve the accuracy and robustness of ICH segmentation, reduce the rate of misdiagnosis and missed diagnosis, and contribute to improving clinical work efficiency and patient treatment. However, in the task of ICH segmentation, multi-class segmentation also has many challenges. ICH usually come in different shapes, sizes, and densities, and there may be different types of bleeding and also patient differences. Therefore, it is necessary to use more training data for multi-class segmentation.

Task 2: Semi-supervised with pixel-labeled and unlabeled data. Acquiring labeled medical imaging data can be a costly and challenging process, whereas unlabeled data is usually more easily accessible. Unfortunately, annotating medical images requires specialized domain expertise, which can pose a significant barrier to the widespread use of deep learning methods in clinical practice. Semi-supervised learning (SSL) addresses this challenge by using a small amount of labeled data and a large amount of unlabeled data for model training. In BHSD, we simulate the SSL scenario by discarding the image-level annotations to build the unlabeled data. This method would be able to combine data with pixel-level annotations and unlabeled data to evaluate the performance of SSL methods.

Task 3: Semi-weakly supervised with pixel-labeled and weakly-labeled data In medical imaging, there is also a wide range of weakly-labeled data, such as CT volumes with slice-level annotations only. This data is collected not only to enable classification tasks, but also to enhance segmentation tasks. Therefore, it is worth developing a combination of existing models with weakly labeled data to achieve better segmentation performance [18,26]. To do this, we derived slice-level annotations from the original RSNA dataset and incorporated these into the reconstructed volumes. This allowed us to explore the contribution of weakly-labeled data on segmentation performance. Experiments conducted on the BHSD show value of using weakly labeled data in clinical settings.

3 Experiments and Benchmarking Methods

In this section, a set of experiments are performed for each task on the BHSD and benchmarks are provided for future model evaluation using this dataset. Due to the nature of the data, the entire data can be divided into three parts for comparison and analysis.

- Supervised segmentation experiments based on pixel-level annotations.
- Semi-supervised experiments using the state of the art (SOTA) model from the supervised experiments, combined with different semi-supervised methods, and unannotated volumes.
- Using SOTA semi-supervised method and SOTA model, combined with weakly-labeled volumes, semi-weakly supervised experiments were conducted under different data distributions.

3.1 Supervised segmentation with advanced backbones.

SOTA backbones. In this task, five models were evaluated on a supervised semantic segmentation task: Unter [7], SwinUnetr [6,16], CoTr [25], nnFormer [28,21], and nnUNet [12]. All five models perform well on routine medical image segmentation tasks, so we used them for supervised experiments on the BHSD.

“Salary-on-costs” you will need to add the casual loading

Table 1. Performance of Supervised Model, measured by Dice similarity coefficient (DSC). Methods based on 3D data include: nnUnet3D, CoTr, nnFormer, UNETR, Swin-UNETR.

Model	EDH	IPH	IVH	SAH	SDH	Mean
Unetr	1.64	28.28	22.08	4.36	3.63	11.99
Swin-Unetr	2.53	34.18	29.28	10.07	8.43	16.89
CoTr	1.63	48.62	53.55	17.88	15.44	27.43
nnFormer	0.00	69.75	25.78	25.94	10.31	29.19
nnUnet3D	4.81	54.12	51.48	21.57	15.23	29.44

Evaluation metrics and results. In the BHSD, the 200 volumes were divided into a training and testing set, each containing 100 volumes. Segmentation performance was evaluated using the Dice similarity coefficient (DSC) [3], which compares the similarity between the predicted and true segmentation. The experimental results are listed in Table 1. We can find that nnUNet achieves SOTA-level segmentation performance with an average DSC over all diseases of 29.44%. We therefore take the performance of nnUNet as an appropriate benchmark and chose this model as the backbone for the remaining experiments.

3.2 Semi-supervised segmentation with unlabeled volumes

SOTA methods. In this task, four methods were applied to this dataset for testing, which were: mean teacher [20], cross pseudo supervision (CPS) [2], entropy minimization [23], and interpolation consistency [22].

The CPS method uses cross pseudo-supervision to improve accuracy by using the pseudo-labels generated by one model to train another model, and then using this new model to generate new pseudo-labels, iterating over this process to improve the accuracy of the pseudo-labelled data and improve the performance of the model segmentation.

Evaluation metrics and results. In these experiments, the 700 volumes were divided into a training and testing set. The training set contains 600 volumes, of which 100 are labeled and 500 are unlabeled data, and the testing set contains 100 volumes. The experimental results are listed in Table 2. We can find that CPS methods achieves SOTA-level segmentation performance, reaching 49.50% DSC in binary segmentation task. We therefore take the performance of CPS method as an appropriate benchmark and chose this method as the basic method for the remaining experiments.

Table 2. Semi-supervised performance based on nnUNet. To highlight the advantages of semi-supervision, we merged all the hemorrhage categories and report foreground and background semantic segmentation results.

Method	unlabeled samples	Dice
SupOnly	0	45.10 \pm 0.21
Entropy Minimization	500	36.91 \pm 0.16
Mean Teacher	500	44.63 \pm 0.18
Interpolation Consistency	500	45.38 \pm 0.33
Cross Pseudo Supervision	500	49.50 \pm 0.19

3.3 Semi-weakly supervised segmentation with weakly-labeled volumes

SOTA methods. In contrast to purely semi-supervised experiments, although the method of semi-supervised training and the structure of the model were not adjusted in this experiment, the experiment was carried out by adjusting the number of bleeding volumes and the number of bleed-free volumes after introducing image-level annotations to the data, which we define as a semi-weakly supervised segmentation task. In this group of experiments, when a considerable number of ICH-free volumes were introduced to the training dataset for comparison experiments, surprisingly, the performance of the model was enhanced %even without such bleeding feature volumes.

Table 3. The Semi-weakly supervised experiment performance under different data distributions was adjusted by image-level annotations. All data for auxiliary enhancement of nnUNet based on CPS method had image-level annotations and were divided into volumes with and without bleeding.

Experiment	Method	bleeding volumes	no bleeding volumes	Dice
1	Sup	0	0	45.10 \pm 0.21
2	CPS	500	0	49.50 \pm 0.19
3	CPS	500	500	48.86 \pm 0.23
4	CPS	500	1000	49.51 \pm 0.20
5	CPS	500	1500	48.84 \pm 0.15
6	CPS	0	1500	48.71 \pm 0.17

Evaluation metrics and results. In these experiments, the 2200 volumes were divided into training and testing sets. The training set consisted of 2100 volumes, including 100 volumes with pixel-level annotations, and 2000 volumes with image-level annotations, of which 1500 don't have ICH. The test dataset is the same as the previous experiment. As shown in Table 3, comparing the results of experiment 1, 2 and 6, it can be found that the data without ICH can effectively improve the performance of the model, and even achieve similar performance with the hemorrhage data.

These results reinforce the notion that the use of negative samples can help reduce overfitting improve generalisation by increasing the diversity and contrast of the data. In particular, with the semi-supervised approach, the inclusion of negative samples improves the learned representations by pushing the negative samples away from the positive ones, thus providing a better decision boundary for the model. Comparing the results of experiments 3, 4, 5 and 6, it was found that the performance of the model was enhanced when using both the non-bleeding and bleeding data alone. However, the performance of the non-bleeding data was not consistent, especially when combining the non-bleeding data with the bleeding data, and a linear increase in the non-bleeding data did not result in a performance gain.

Overall, our results indicate that volumes without ICH can also be effectively employed for semi-supervised tasks, highlighting that an appropriate amount of such data can be utilized to enhance model performance, when annotated data is limited.

4 Conclusion

In this paper, we describe a 3D CT head dataset for intracranial hemorrhage segmentation. This dataset includes a diverse mix of head scans with pixel-level and slice-level annotations, as well as scans with and without hemorrhage. To qualitatively and quantitatively scrutinize the characteristics of the BHSD, we compare popular SOTA models and diverse training techniques and draw three conclusions from our study. Firstly, the BHSD can significantly enhance the performance of SOTA models for multi-class segmentation of ICH. Secondly, the BHSD improves model performance using a semi-supervised approach even when the volumes are not annotated at the pixel-level. Finally, by incorporating the weakly-labeled data from the BHSD, the no bleed data can also be utilized to enhance segmentation performance. Hence, the BHSD is a valuable dataset for ICH segmentation models, facilitating the development and validation of computer-aided diagnosis in clinical practice.

Tasks in the field of general vision and medical image processing are often quite different, especially in terms of the amount and quality of data. The amount of data available in medical imaging is usually much smaller than in general-purpose computer vision, while the quality of the data is more critical. Medical image data usually needs to be collected by professional instruments, and their quality may be affected by different factors, such as noise, artifacts, etc. Despite this, in certain clinical scenarios, a large number of unlabeled and weakly labeled data can be collected. If this part of data can be fully utilized, the problem of limited data will be greatly alleviated. Throughout extensive experiments, this paper discovers that semi-supervised approaches can leverage *non-bleeding* scans to improve performance. Our BHSD exploits this insight and offers a large volumes of non-bleeding scans for advancing future segmentation techniques. This is where the value of BHSD comes in, providing an opportunity for medical image analysis techniques to study how segmentation tasks can make better use

of unlabeled and weakly labeled volumes that are widely available in medical Settings.

References

1. Auer, L.M., Deinsberger, W., Niederkorn, K., Gell, G., Kleinert, R., Schneider, G., Holzer, P., Bone, G., Mokry, M., Körner, E., et al.: Endoscopic surgery versus medical treatment for spontaneous intracerebral hematoma: a randomized study. *Journal of neurosurgery* **70**(4), 530–535 (1989)
2. Chen, X., Yuan, Y., Zeng, G., Wang, J.: Semi-supervised semantic segmentation with cross pseudo supervision. In: *Proceedings of the IEEE/CVF Conference on Computer Vision and Pattern Recognition*. pp. 2613–2622 (2021)
3. Dice, L.R.: Measures of the amount of ecologic association between species. *Ecology* **26**(3), 297–302 (1945)
4. Flanders, A.E., Prevedello, L.M., Shih, G., Halabi, S.S., Kalpathy-Cramer, J., Ball, R., Mongan, J.T., Stein, A., Kitamura, F.C., Lungren, M.P., et al.: Construction of a machine learning dataset through collaboration: the rsna 2019 brain ct hemorrhage challenge. *Radiology: Artificial Intelligence* **2**(3), e190211 (2020)
5. Grønbæk, H., Johnsen, S.P., Jepsen, P., Gislum, M., Vilstrup, H., Tage-Jensen, U., Sørensen, H.T.: Liver cirrhosis, other liver diseases, and risk of hospitalisation for intracerebral haemorrhage: a danish population-based case-control study. *BMC gastroenterology* **8**, 1–6 (2008)
6. Hatamizadeh, A., Nath, V., Tang, Y., Yang, D., Roth, H.R., Xu, D.: Swin unetr: Swin transformers for semantic segmentation of brain tumors in mri images. In: *Brainlesion: Glioma, Multiple Sclerosis, Stroke and Traumatic Brain Injuries: 7th International Workshop, BrainLes 2021, Held in Conjunction with MICCAI 2021, Virtual Event, September 27, 2021, Revised Selected Papers, Part I*. pp. 272–284. Springer (2022)
7. Hatamizadeh, A., Tang, Y., Nath, V., Yang, D., Myronenko, A., Landman, B., Roth, H.R., Xu, D.: Unetr: Transformers for 3d medical image segmentation. In: *Proceedings of the IEEE/CVF winter conference on applications of computer vision*. pp. 574–584 (2022)
8. Hemphill III, J.C., Greenberg, S.M., Anderson, C.S., Becker, K., Bendok, B.R., Cushman, M., Fung, G.L., Goldstein, J.N., Macdonald, R.L., Mitchell, P.H., et al.: Guidelines for the management of spontaneous intracerebral hemorrhage: a guideline for healthcare professionals from the american heart association/american stroke association. *Stroke* **46**(7), 2032–2060 (2015)
9. Howard, G., Cushman, M., Howard, V.J., Kissela, B.M., Kleindorfer, D.O., Moy, C.S., Switzer, J., Woo, D.: Risk factors for intracerebral hemorrhage: the reasons for geographic and racial differences in stroke (regards) study. *Stroke* **44**(5), 1282–1287 (2013)
10. Hssayeni, M., Croock, M., Salman, A., Al-khafaji, H., Yahya, Z., Ghoraani, B.: Computed tomography images for intracranial hemorrhage detection and segmentation. *Intracranial Hemorrhage Segmentation Using A Deep Convolutional Model. Data* **5**(1), 14 (2020)
11. Isaka, S., Kawanaka, H., Aronow, B.J., Prasath, V.S.: Multi-class segmentation of lung immunofluorescence confocal images using deep learning. In: *2019 IEEE International Conference on Bioinformatics and Biomedicine (BIBM)*. pp. 2362–2368. IEEE (2019)

12. Isensee, F., Jaeger, P.F., Kohl, S.A., Petersen, J., Maier-Hein, K.H.: nnu-net: a self-configuring method for deep learning-based biomedical image segmentation. *Nature methods* **18**(2), 203–211 (2021)
13. Larobina, M., Murino, L.: Medical image file formats. *Journal of digital imaging* **27**, 200–206 (2014)
14. Lee, H., Kim, M., Do, S.: Practical window setting optimization for medical image deep learning. arXiv preprint arXiv:1812.00572 (2018)
15. Li, X., Luo, G., Wang, K., Wang, H., Li, S., Liu, J., Liang, X., Jiang, J., Song, Z., Zheng, C., et al.: The state-of-the-art 3d anisotropic intracranial hemorrhage segmentation on non-contrast head ct: The instance challenge. arXiv preprint arXiv:2301.03281 (2023)
16. Liu, Z., Lin, Y., Cao, Y., Hu, H., Wei, Y., Zhang, Z., Lin, S., Guo, B.: Swin transformer: Hierarchical vision transformer using shifted windows. In: *Proceedings of the IEEE/CVF international conference on computer vision*. pp. 10012–10022 (2021)
17. McCarron, M.O., Nicoll, J.A., Ironside, J.W., Love, S., Alberts, M.J., Bone, I.: Cerebral amyloid angiopathy-related hemorrhage: Interaction of apoe ϵ 2 with putative clinical risk factors. *Stroke* **30**(8), 1643–1646 (1999)
18. Reiß, S., Seibold, C., Freytag, A., Rodner, E., Stiefelhagen, R.: Graph-constrained contrastive regularization for semi-weakly volumetric segmentation. In: *Computer Vision–ECCV 2022: 17th European Conference, Tel Aviv, Israel, October 23–27, 2022, Proceedings, Part XXI*. pp. 401–419. Springer (2022)
19. Steiner, T., Salman, R.A.S., Beer, R., Christensen, H., Cordonnier, C., Csiba, L., Forsting, M., Harnof, S., Klijn, C.J., Krieger, D., et al.: European stroke organisation (eso) guidelines for the management of spontaneous intracerebral hemorrhage. *International journal of stroke* **9**(7), 840–855 (2014)
20. Tarvainen, A., Valpola, H.: Mean teachers are better role models: Weight-averaged consistency targets improve semi-supervised deep learning results. *Advances in neural information processing systems* **30** (2017)
21. Vaswani, A., Shazeer, N., Parmar, N., Uszkoreit, J., Jones, L., Gomez, A.N., Kaiser, L., Polosukhin, I.: Attention is all you need. *Advances in neural information processing systems* **30** (2017)
22. Verma, V., Kawaguchi, K., Lamb, A., Kannala, J., Solin, A., Bengio, Y., Lopez-Paz, D.: Interpolation consistency training for semi-supervised learning. *Neural Networks* **145**, 90–106 (2022)
23. Vu, T.H., Jain, H., Bucher, M., Cord, M., Pérez, P.: Advent: Adversarial entropy minimization for domain adaptation in semantic segmentation. In: *Proceedings of the IEEE/CVF Conference on Computer Vision and Pattern Recognition*. pp. 2517–2526 (2019)
24. Wang, X., Shen, T., Yang, S., Lan, J., Xu, Y., Wang, M., Zhang, J., Han, X.: A deep learning algorithm for automatic detection and classification of acute intracranial hemorrhages in head ct scans. *NeuroImage: Clinical* **32**, 102785 (2021)
25. Xie, Y., Zhang, J., Shen, C., Xia, Y.: Cotr: Efficiently bridging cnn and transformer for 3d medical image segmentation. In: *Medical Image Computing and Computer Assisted Intervention–MICCAI 2021: 24th International Conference, Strasbourg, France, September 27–October 1, 2021, Proceedings, Part III 24*. pp. 171–180. Springer (2021)
26. Yap, B.P., Ng, B.K.: Semi-weakly supervised contrastive representation learning for retinal fundus images. arXiv preprint arXiv:2108.02122 (2021)

27. Yushkevich, P.A., Gerig, G.: Itk-snap: an intractive medical image segmentation tool to meet the need for expert-guided segmentation of complex medical images. *IEEE pulse* **8**(4), 54–57 (2017)
28. Zhou, H.Y., Guo, J., Zhang, Y., Yu, L., Wang, L., Yu, Y.: nnformer: Interleaved transformer for volumetric segmentation. *arXiv preprint arXiv:2109.03201* (2021)